LARGE SCALE STRUCTURE

14.1 Overview

The Universe around us is isotropic only on very large scales, of order 100s of Mpc. On smaller scales—from galaxies which have a density $\sim 10^5 - 10^6$ times higher than the mean, to superclusters of galaxies and voids—the universe exhibits a great deal of structure (see Fig. 14.1).

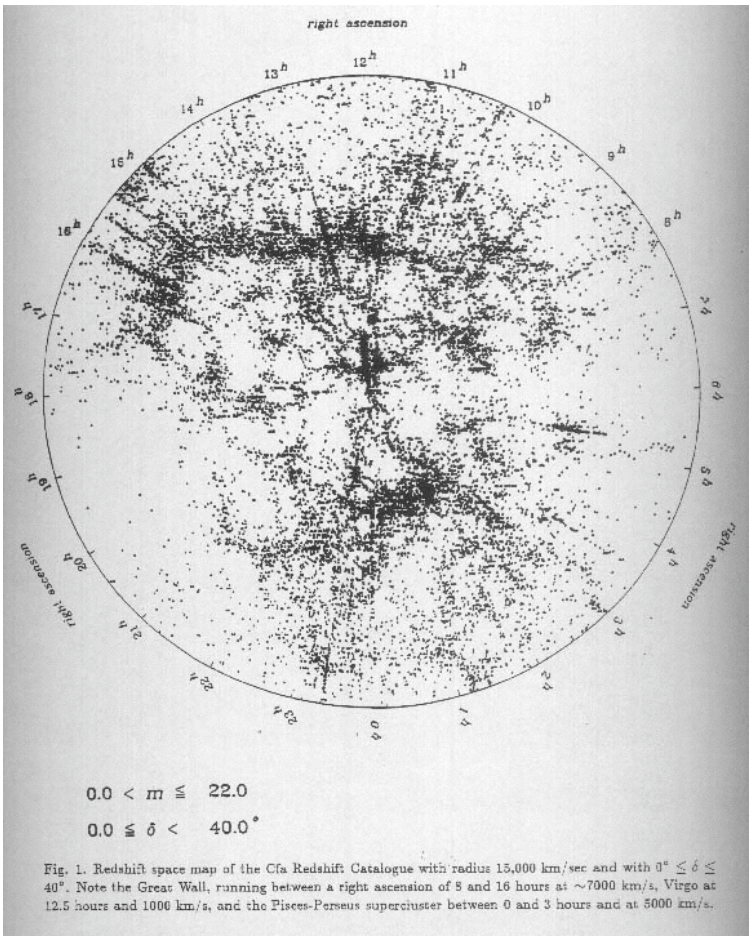

Figure 14.1: One of the earliest pictures of the large scale structure in the galaxy distribution is the slice made from the Center for Astrophysics redshift survey of galaxies brighter than $B \simeq 15.5$ and with velocities $v < 12\,000\,\mathrm{km\ s^{-1}}$ ($z \leq 0.04$). The plane of our own Galaxy runs across the sky from right ascension 6^h to 19^h. This band is devoid of galaxies in the plot because the Milky Way gets in the way. Note the large scale features like the 'Great Wall' between 8^h and 16^h, and the empty 'voids' .

The existence of these cosmological structures tells us something important about the initial conditions of the Big Bang, and about the physical processes which have operated subsequently. In general, structure will develop differently in different cosmological models; an example is shown in Fig. 14.2. Thus, from a statistical description of the large scale structure of the Universe we can deduce the best-fitting values of some cosmological parameters (primarily $\Omega_{\mathrm{m},0}$, $\Omega_{\mathrm{b},0}$, H_0, and the primordial spectral index n (to be defined later).

Nowadays, sophisticated hydrodynamical simulations performed on some of the most powerful computers available to astronomers allow the growth of cosmic structure to be followed from high redshift to the present time. By varying the initial conditions and following the subsequent evolution in the distribution of galaxies and dark matter, it is possible to determine the set of cosmological parameters (and baryon physics) that best fit the real Universe. Some examples can be found here:
`http://www.mpa-garching.mpg.de/galform/data_vis/`.

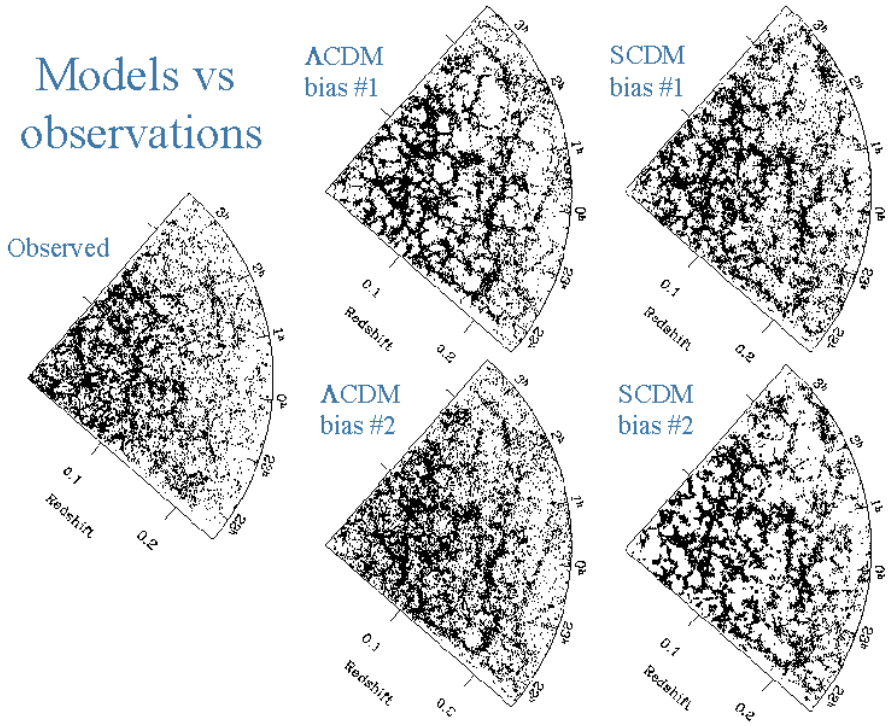

Figure 14.2: A pictorial example of how the large scale structure in the distribution of galaxies can be used to discriminate between different model universes. Just from visual inspection, three of the four models can be ruled out.

14.1.1 Primordial Fluctuations

The working hypothesis is that tiny perturbations were present at early times and that these primordial density fluctuations subsequently grew through self-gravity and other effects, and developed into the structures we see today. Two candidates for what might have initially seeded the structure are:

1. Amplification of quantum zero-point fluctuations during an inflationary era (Heisenberg's uncertainty principle guarantees that, because the positions of particles are indeterminate, there must have been density inhomogeneities in the early universe).
2. Topological defects formed in a cosmological phase transition.

Consider an initial density perturbation defined by the dimensionless parameter:

$$1 + \delta(\mathbf{x}) \equiv \rho(\mathbf{x})/\langle\rho\rangle \tag{14.1}$$

where, as usual, we use the symbol ρ to indicate the density. With the density content divided into nonrelativistic matter and radiation, there are two distinct perturbation modes, with different relations between the two density components.

Imagine starting with a uniform distribution of matter and radiation; the simplest way to perturb the density would be to compress (or expand) a region within the volume adiabatically. This would change the matter density and the photon number density by the same factor. But the energy density of matter and radiation respond differently to a change in scale factor a—or equivalently temperature T [recall that for pressureless matter $\rho_{\rm m} \propto 1/a^3$ (eq. 2.18), while for radiation $\rho_{\rm rad} \propto 1/a^4$ (eq. 2.23)]. Thus, **adiabatic perturbations** would change the energy density of matter and radiation differently: $\delta_{\rm rad} = 4\delta_{\rm m}/3$.

The second mode perturbs the entropy density but not the energy density. The resulting fluctuations are termed **isocurvature perturbations**—since the total energy density remains homogeneous, there is no perturbation to the spatial curvature and $\rho_{\rm rad}\delta_{\rm rad} = -\rho_{\rm m}\delta_{\rm m}$. You could think, for example, of variations in the relative fraction of baryons to photons.

At very early times, when the universe is strongly dominated by radiation, isocurvature initial conditions effectively correspond to a vanishingly small fractional perturbation in the radiation density, with only the matter density varying significantly.

Now, let's imagine that we wanted to create a non-uniform density field at some given time in the history of the universe. Isocurvature perturbations would be more natural on causality arguments (it would be impossible to change the mean density on scales larger than the horizon at that time). This is indeed the case in models involving a late-time cosmological phase transition—such as the topological defect models mentioned earlier.

However, inflation changes the nature of the particle horizon at early times. Thus, in inflationary models, fluctuations in total density can be produced on scales which vastly exceed c/H_0. If these curvature fluctuations are generated prior to the processes responsible for the baryon asymmetry of the Universe, then adiabatic modes will be the norm.

14.1.2 The Transfer Function

Any primordial density perturbations will subsequently be modified by a variety of physical processes: growth under self-gravitation, the effect of pressure, and dissipative processes. This evolution works in the sense that modes of short wavelength have their amplitudes reduced relative to those of long wavelength. The overall effect is encapsulated in the **transfer function**

$$T_k \equiv \frac{\delta_k(z=0)}{\delta_k(z)D(z)}$$

where $D(z)$ is the linear growth factor between redshift z and the present. The form of the transfer function depends on the type of fluctuation (adiabatic or isocurvature) and on the matter content of the universe: models in which the contribution to $\Omega_{\rm m}$ is from baryons, cold dark matter, hot dark matter, or a mixture of any of these, all have different transfer functions.

Linear (by which we mean $|\Delta\rho|/\langle\rho\rangle \ll 1$) adiabatic perturbations grow with time as follows:

$$\delta \propto \begin{cases} a^2 & \text{in the radiation dominated era} \\ a & \text{in the matter dominated era} \end{cases} \tag{14.2}$$

We can see this most easily in a flat ($k = 0$) FRW model, where:

$$H^2 = \frac{8\pi G}{3}\,\rho \tag{14.3}$$

with $\rho = \rho_{\rm tot} = \rho_{\rm crit}$. A spherical region of enhanced density $\rho' > \rho$ within this flat universe will also expand with the same Hubble law if its size exceeds the particle horizon and its particles are therefore not causally connected. Because the dynamics of the spherical density fluctuation depend only on the mass contained within (recall Birkhoff's theorem), it evolves as a separate entity, like a miniature closed universe, according to:

$$H^2 = \frac{8\pi G}{3}\,\rho' - \frac{kc^2}{a^2}\,, \tag{14.4}$$

with $k > 0$. Subtracting one equation from the other, we find

$$\delta \equiv \frac{\rho' - \rho}{\rho} = \frac{3}{8\pi G}\,\frac{kc^2}{a^2}\,\frac{1}{\rho} \tag{14.5}$$

The evolution of δ is hence related to the evolution of the curvature kc^2/a^2 relative to the density ρ. In a matter dominated universe $\rho \propto a^{-3}$ and in a radiation dominated universe $\rho \propto a^{-4}$ and hence

$$\delta \propto \frac{a^{-2}}{\rho} \propto \begin{cases} a^2 & \text{in the radiation dominated era} \\ a & \text{in the matter dominated era} \end{cases} \tag{14.2}$$

Recalling that $a \propto t^{1/2}$ in a radiation dominated universe, and $a \propto t^{2/3}$ in a matter dominated universe, we deduce

$$\delta = \delta_i \cdot \begin{cases} t/t_i & \text{in the radiation dominated era} \\ (t/t_i)^{2/3} & \text{in the matter dominated era} \end{cases} \tag{14.6}$$

The amplitude of our super-horizon adiabatic fluctuation therefore increased linearly with time during the radiation era and only a little more slowly during the matter-dominated era. Note that the increase in $\delta\rho/\rho$ did *not* involve the separation of the high-density region from the Hubble flow, but is just due to the difference in the rates at which the density decreased inside and outside the fluctuation as the universe expanded.

Isocurvature perturbations to the matter, on the other hand, evolve as:

$$\delta_{\rm m} \propto \begin{cases} \text{constant} & \text{in the radiation dominated era} \\ a^{-1} & \text{in the matter dominated era} \end{cases} \tag{14.7}$$

In the adiabatic case, gravity causes the mode amplitude to increase; in the isocurvature case the evolution acts to preserve the initial uniform density. Thus, isocurvature perturbations act as a 'deep freeze' preserving potential density fluctuations and protecting them from the dissipation processes suffered by the adiabatic fluctuations (which we shall discuss presently). In both cases, the shape of the primordial perturbation spectrum is preserved, and only its amplitude changes with time.

On small scales, however, a variety of physical processes affect the way perturbations grow:

1. **Pressure** opposes gravity effectively for wavelengths below the Jeans length:

$$\lambda_J = c_s \sqrt{\frac{\pi}{G\rho}}$$

On scales smaller than the Jeans length, where pressure forces dominate over gravitational forces, the fluctuations move as sound waves in the fluid, damped by its viscosity and transporting energy from one region of space to another. In the radiation era, $c_{\rm s} = c/\sqrt{3}$ and so the Jeans length is always close to the size of the horizon. It reaches a maximum value at the matter-radiation equality, when the sound speed begins to drop. This defines an important scale, the comoving horizon size at $z_{\rm eq}$:

$$r_H(z_{\rm eq}) \simeq \frac{16}{\Omega_{\rm m,0} h^2}\,{\rm Mpc}$$

Beyond this scale, perturbations should be affected by gravity only and we would then expect to see a bend in the spectrum of perturbations where pressure starts to become important. Notice that this scale depends on $\Omega_{\rm m,0}$; so here is an example of how the galaxy distribution can be used to determine cosmological parameters.

The Jeans analysis assumes a tightly coupled baryon-photon plasma. There are two situations where this is inappropriate.

2. **Photon Diffusion**. At early times the plasma is very optically thick, but as the universe expands the mean free path for photons increases and the photons tend to leak out of the sound waves and then damp out, smoothing the inhomogeneities in the photon-baryon fluid. This is the *Silk damping* we already discussed in Lecture 10.4.2. At the epoch of last scattering, fluctuations on scales smaller than the distance travelled by the photon random walk:

$$\lambda_s = 2.7\,(\Omega_{\mathrm{m},0}\Omega_{\mathrm{b},0}^2 h^6)^{-1/4}\,\mathrm{Mpc}$$

have been damped out. Nowadays the Silk damping of acoustic fluctuations is not thought to be so critical: the major contributor to Ω_{m} is dark matter, and the baryons can fall into the dark matter potential wells after last scattering.

3. **Free Streaming**. At early times, dark matter particles will undergo free streaming at the speed of light, and so erase all scales up to the horizon, a process which only stops when the particles go non-relativistic. For massive neutrinos this happens at z_{eq} (because the number densities of photons and neutrinos are comparable).

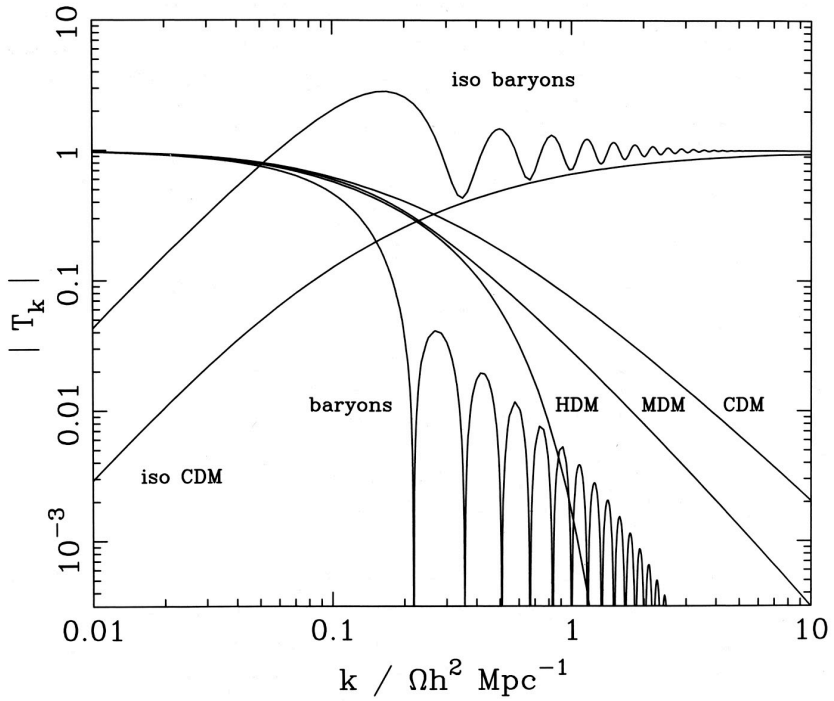

Figure 14.3: (Reproduced from J. Peacock's *Physical Cosmology*) A plot of transfer functions for various models. For adiabatic models, $T_k \to 1$ at small k, whereas the opposite is true for isocurvature models. A number of possible matter contents are illustrated: pure baryons,; pure C(old)DM; pure H(ot)DM; M(ixed)DM (30% HDM, 70% CDM).

14.2 Measures of Large Scale Structure

Since the pioneering work by John Huchra and colleagues at the CfA in the 1980s, galaxy surveys have proliferated and have reached further and further into the distant Universe (see Figure 14.4). Hundreds of galaxy redshifts can now be measured simultaneously thanks to technological advances in the size of astronomical detectors and in efficient, multiplexing spectrographs.

One of the aims of all of these large surveys is to analyse the large scale distribution of galaxies and thereby determine both the form of the initial spectrum of fluctuations, and the transfer function—with its encoded cosmological parameters—which has turned them into the structures we see today.

In order to interpret the results of these extensive galaxy surveys, we need a mathematical description of the statistical properties of the distribution of galaxies. The analogy with waves on the surface of a lake may

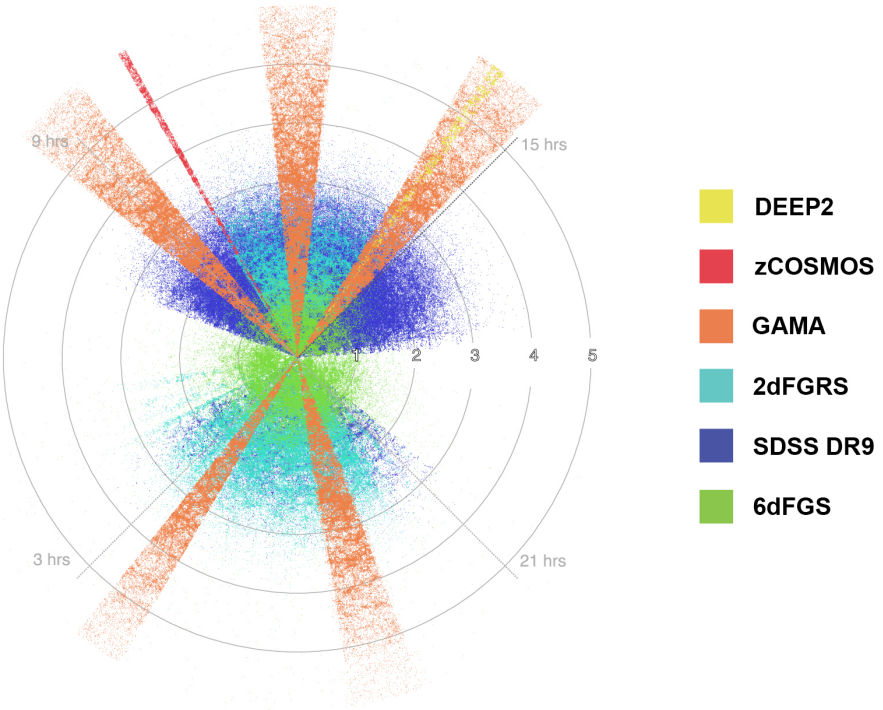

Figure 14.4: Illustration of the depth and sky coverage of some of the most extensive recent galaxy surveys. The integers on the positive x-axis indicate the look-back time in Gyr. The DEEP2, zCOSMOS and GAMA surveys extend to well beyond $z = 0.6$, more than ~ 20 times further than the pioneering CfA surveys of the 1980s.

be helpful here. Their statistical properties, such as the distributions of wavelengths and amplitudes, depend on the shape and depth of the lake and the strength and direction of the wind blowing over the surface. If we assume that the wind is constant with time, then the statistical properties of the surface of the lake would not change. This doesn't of course mean that two snapshots of the lake taken at different times would look identical, but rather that they are statistically indistinguishable—there is no way of deciding which of the two snapshot was taken first.

The most common mathematical tool used to describe the statistical properties of the large scale distribution of matter is Fourier analysis.

14.2.1 Fourier transforms of the density field

We start with our dimensionless density perturbation field:

$$\delta(\mathbf{x}) \equiv \frac{\rho(\mathbf{x}) - \langle\rho\rangle}{\langle\rho\rangle} \tag{14.8}$$

which we can think of as the superposition of many modes. In a flat comoving geometry, a field such as this is most conveniently described with Fourier analysis.[1] But how do we make a Fourier expansion of the density field in an infinite universe? Imagine that the field is periodic within a box of side L; then we would just have a sum over the wave modes:

$$F(\mathbf{x}) = \sum F_{\mathbf{k}} e^{-i\mathbf{k}\cdot\mathbf{x}}$$

The requirement of periodicity restricts the allowed wavenumbers to harmonic boundary conditions

$$k_x = n\frac{2\pi}{L}\,, \quad n = 1, 2, \ldots$$

and similarly for k_y and k_z. If we now let the box become arbitrarily large, then the sum will become an integral that incorporates the density of states in k-space. The Fourier relations in n dimensions are thus

$$F(x) = \left(\frac{L}{2\pi}\right)^n \int F_k(k)\, e^{-i\mathbf{k}\cdot\mathbf{x}}\, d^n k$$

[1] In other geometries, the correct approach is to consider the eigenfunctions of the wave equation in curved space. Normally this complication is neglected because even in an open universe, the difference becomes significant only on scales of the order of the present-day horizon.

$$F_k(k) = \left(\frac{1}{L}\right)^n \int F(x)\, e^{i\mathbf{k}\cdot\mathbf{x}}\, d^n x$$

In particular, in three dimensions the forward and inverse Fourier transforms then are:

$$F(\mathbf{x}) = V \int \frac{d^3k}{(2\pi)^3}\, F(\mathbf{k})\, e^{-i\mathbf{k}\cdot\mathbf{x}} \tag{14.9}$$

and

$$F(\mathbf{k}) = \frac{1}{V} \int d^3x\, F(\mathbf{x})\, e^{i\mathbf{k}\cdot\mathbf{x}} \tag{14.10}$$

where V is the volume.

14.2.2 The galaxy (auto)correlation function

A commonly used measure of clustering is the second moment of the density field:

$$\xi(\mathbf{r}) \equiv \langle \delta(\mathbf{x}) \cdot \delta(\mathbf{x}+\mathbf{r}) \rangle \tag{14.11}$$

which is called the autocorrelation function of the density field—usually referred to simply as the correlation function. The angular brackets indicate an averaging over the normalization volume V. Before deriving the Fourier formulation of $\xi(\mathbf{r})$, let us consider briefly its meaning. If galaxies were distributed uniformly through space, with number density n, then the

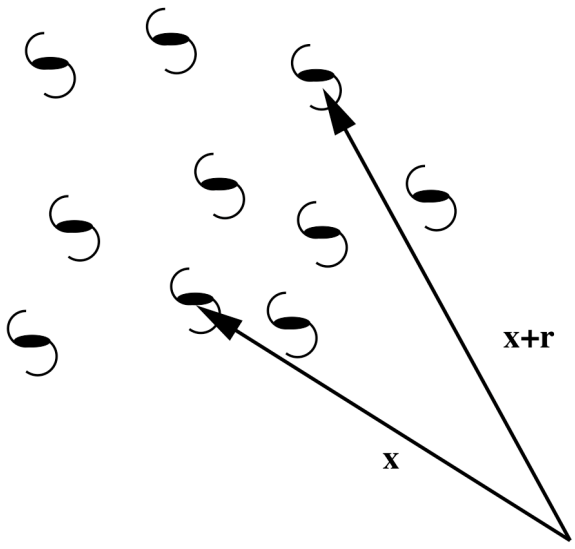

Figure 14.5: Density correlation measurement

probability dP of finding a galaxy within a volume dV would be the same everywhere, $dP = n\,dV$.[2] However, in reality galaxies are clustered, so that the probability of finding a galaxy within a volume dV at a distance $\mathbf{r}$ from a specified galaxy becomes:

$$dP = n[1 + \xi(\mathbf{r})]dV \tag{14.12}$$

where n is the average number density of galaxies and $\xi(\mathbf{r})$ is the two-point (or galaxy-galaxy) correlation function which describes whether galaxies are more concentrated ($\xi > 0$) or more dispersed ($\xi < 0$) than average (see Fig. 14.5). Note that with the definition of (14.11), $\xi(\mathbf{r})$ measures equally well the clustering of voids (underdense regions where $\delta(\mathbf{x}) < 0$).

In Fourier space, we can express ξ as the sum:

$$\xi = \left\langle \sum_{\mathbf{k}} \sum_{\mathbf{k}'} \delta_{\mathbf{k}} \delta^*_{\mathbf{k}'}\, e^{i(\mathbf{k}'-\mathbf{k})\cdot\mathbf{x}}\, e^{-i\mathbf{k}\cdot\mathbf{r}} \right\rangle \tag{14.13}$$

where we have used the relation between modes with opposite wavevectors that holds for any real field: $\delta_{\mathbf{k}}(-\mathbf{k}) = \delta^*_{\mathbf{k}}(\mathbf{k})$ (where δ^* is the complex conjugate of δ). Now, by the periodic boundary conditions, all the cross terms with $\mathbf{k}' \neq \mathbf{k}$ average to zero; thus, the double sum in (14.13) reduces to the integral:

$$\xi(\mathbf{r}) = \frac{V}{(2\pi)^3} \int |\delta_{\mathbf{k}}|^2\, e^{-i\mathbf{k}\cdot\mathbf{r}}\, d^3k \tag{14.14}$$

In short, the correlation function is the Fourier transform of the power spectrum (cfr. eq. 14.9) for which the alternative notation:

$$P(k) \equiv \langle |\delta_k|^2 \rangle \tag{14.15}$$

is often used. Since in an isotropic universe the density perturbation spectrum contains no preferred direction, we have the isotropic power spectrum: $\langle |\delta_{\mathbf{k}}|^2(\mathbf{k}) \rangle = |\delta_k|^2(k)$. The angular part of the k-space integral in (14.14) can therefore be performed immediately. We introduce spherical polar coordinates with the polar axis along $\mathbf{k}$, and use the fact that ξ is real—so

[2] We assume that dV is sufficiently small that $dP \leq 1$.

that $e^{-i\mathbf{k}\cdot\mathbf{r}} \rightarrow \cos(kr\cos\theta)$. This yields:

$$\xi(r) = \frac{V}{(2\pi)^3}\int dk\, k^2 \int_0^{2\pi} d\phi \int_{-1}^{1} d(\cos\theta) P(k)\cos(kr\cos\theta) \qquad (14.16)$$

from which we obtain

$$\xi(r) = \frac{V}{(2\pi)^3}\int P(k)\,\frac{\sin kr}{kr}\,4\pi k^2 dk \qquad (14.17)$$

It is sometimes convenient to express the power spectrum in dimensionless form, as the variance per logarithmic interval in k :$\Delta^2(k) = d\langle\delta^2\rangle/d\ln k \propto k^3\,P(k)$ [to see this, just consider $\int k^2 dk = \int \frac{k^3}{k} dk = \int k^3 d\ln k$].

So, we define:

$$\Delta^2(k) \equiv \frac{V}{(2\pi)^3}\,4\pi k^3 P(k) \qquad (14.18)$$

Recalling eq. 14.10, we have:

$$\Delta^2(k) = \frac{V}{(2\pi)^3}\,4\pi k^3 \times \frac{1}{V}\int d^3r\,\xi(\mathbf{r})\,e^{i\mathbf{k}\cdot\mathbf{r}}$$

$$\Delta^2(k) = \frac{V}{(2\pi)^3}\,4\pi k^3 \times \frac{4\pi}{V}\int \xi(r)\frac{\sin kr}{kr} r^2 dr$$

(see eq. 14.16), from which we then obtain:

$$\Delta^2(k) = \frac{2}{\pi}k^3 \int_0^{\infty} \xi(r)\frac{\sin kr}{kr}\,r^2\,dr \qquad (14.19)$$

This formulation gives a more intuitive meaning to the power spectrum than $P(k)$, which is a functional representation of the power per unit volume in k-space. For example, $\Delta^2(k) = 1$ means that there are order-unity density fluctuations from modes in the logarithmic bin around wavenumber k. Thus $\Delta^2(k)$ is the natural choice for a Fourier-space counterpart to the dimensionless quantity $\xi(r)$.

14.3 The Spectrum of Fluctuations

Clearly, the power spectrum of density fluctuations is a fundamental quantity in cosmology, but what do we know about its functional form? The

simplest assumption is that the spectrum does not contain any preferred length scale—we do not know of a physical theory which would explain such a feature. Inflationary models quite naturally predict a scale-free spectrum of primordial fluctuations of the form:

$$\langle |\delta_k|^2 \rangle \propto k^n \tag{14.20}$$

where the spectral index n governs the balance between large- and small-scale power. The meaning of different values of n can be appreciated by imagining the results of filtering the density field by passing over it a box of some characteristic moving size x and averaging the density over the box. This will filter out waves with $k > 1/x$, leaving a variance:

$$\langle \delta^2 \rangle \propto \int_0^{1/x} k^n 4\pi k^2 \, dk \;\; \propto x^{-(n+3)} \tag{14.21}$$

In terms of the mass $M \propto x^3$ we then have

$$\delta_{\rm rms} = \sqrt{\langle \delta^2 \rangle} \;\; \propto M^{-(n+3)/6} \tag{14.22}$$

Similarly, as we show below, a power-law spectrum implies a power-law correlation function:

$$\xi(r) = \left(\frac{r}{r_0} \right)^{-\gamma} \tag{14.23}$$

with $\gamma = n + 3$. Notice (from eq. 14.12) that r_0 is the distance from a galaxy at which the probability of finding another galaxy is twice what it would be if galaxies were distributed evenly on the sky. Thus, r_0 is a convenient measure of the clustering length scale.

To see that a power-law spectrum implies a power-law correlation function, recall eq. 14.19:

$$\Delta^2(k) = \frac{2}{\pi} k^3 \int_0^\infty \xi(r) \frac{\sin kr}{kr} \, r^2 \, dr$$

Now substitute $\xi(r) = (r/r_0)^{-\gamma}$

$$\Delta^2(k) = \frac{2k^2 r_0^\gamma}{\pi} \int r^{1-\gamma} \, \sin kr \, dr$$

Looking up the solution to the integral we find:

$$\Delta^2(k) = \frac{2}{\pi}(kr_0)^\gamma \, \Gamma(2-\gamma) \, \sin\frac{(2-\gamma)\pi}{2} \; = \beta(kr_0)^\gamma \tag{14.24}$$

valid for $\gamma < 3$ ($n < 0$).

Let's look at the possible range of values of n. Clearly, our assumption that the Universe be homogeneous on large scales, requires $n > -3$, so that the variance $\langle\delta^2\rangle$ decreases as x increases in eq. 14.21 (or, alternatively, we require $\xi(r) \to 0$ at very large r; hence $\gamma > 0$ in eq. 14.23). The value $n = 0$ means the same power on all scales, or what is sometimes referred to as *white noise*. You would obtain such a power spectrum if you threw down a large number of point masses at random. This is also known as the Poissonian power spectrum because it corresponds to fluctuations between different cells that scale as $1/\sqrt{M_{\rm cell}}$.

The measured galaxy correlation function (see Fig. 14.6) is consistent with a power law of the form:

$$\xi_g(r) \simeq \left(\frac{r}{5\,h^{-1}\,{\rm Mpc}}\right)^{-1.8} \tag{14.25}$$

which corresponds to $n \simeq -1.2$, although r_0 (but not γ) also depends on galaxy type: red (elliptical) galaxies tend to be more clustered than blue (spiral) galaxies, perhaps because they formed earlier, or because ellipticals are formed by mergers (which are more frequent when galaxies are heavily clustered).

Most important of all is the **scale-invariant spectrum** (also known as the Zeldovich, or Harrison-Zeldovich spectrum) which corresponds to $n = 1$. A spectral index of 1 has important consequences. If we consider a perturbation $\delta\Phi$ in the gravitational potential, from the Poisson equation:

$$\nabla^2\delta\Phi = 4\pi G\rho_0\delta\,;$$

in Fourier space we have:

$$\delta\Phi_k = -4\pi G\rho_0\delta_k/k^2$$

that is:

$$\delta\Phi_k \propto \frac{\delta_k}{k^2} \; \propto k^{-3/2}\,.$$

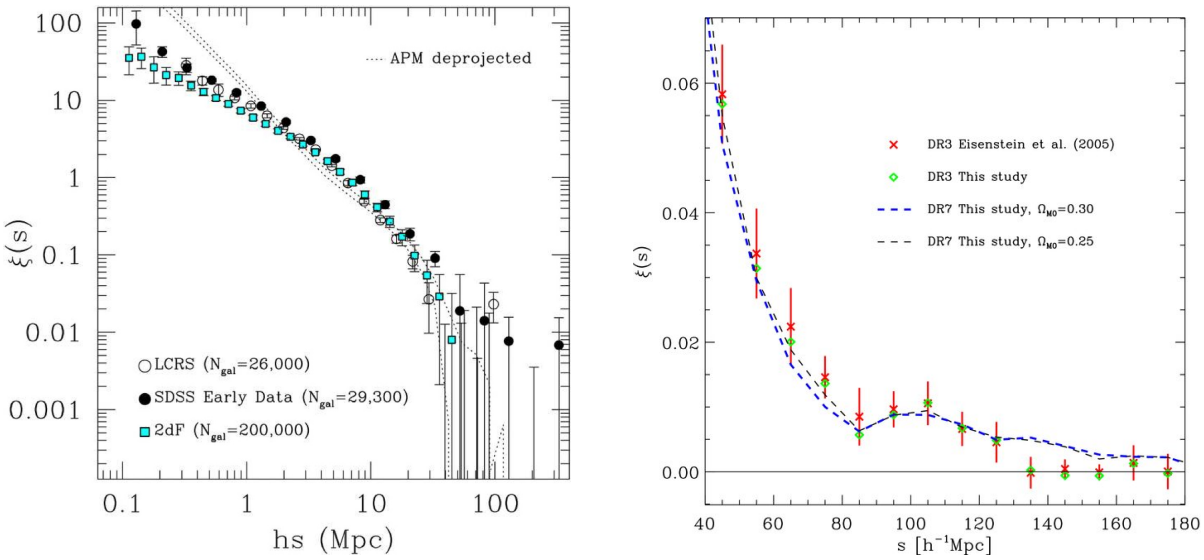

Figure 14.6: *Left:* The galaxy two-point correlation function ($\xi(r)$ in our notation) measured from the near-completed two-degree Field (2dF) galaxy redshift survey is compared with earlier measurements from the Las Campanas Redshift Survey (LCRS) and the first data from the Sloan Digital Sky Survey (SDSS). (Figure reproduced from http://www.roe.ac.uk/∼jap/2df). *Right:* The correlation function of Luminous Red Galaxies (LRGs) on large scales ($60h^{-1}\,\mathrm{Mpc} < s < 400h^{-1}\,\mathrm{Mpc}$, where the 2dF sampling in the left panel is poor) determined from the third and seventh SDSS data releases (DR3 and DR7; figure reproduced from Kazin et al. 2010).

Since $\Delta^2(k) \propto k^3\delta_k^2$ (eq. 14.18), for $n = 1$ we have $\Delta^2(k) \propto k^4$ and

$$\Delta_\Phi^2 \propto \delta\Phi_k^2 k^3 = \text{ constant}$$

Since potential perturbations govern the flatness of spacetime, a scale-invariant spectrum corresponds to a metric that is fractal: spacetime has the same degree of 'wrinkles' on each resolution scale. A scale-invariant spectrum with $n = 1$ (approximately) is one of the predictions of inflationary theories and appears to be confirmed by observations of $P(k)$ on the largest scales as measured by the temperature anisotropies of the CMB.

14.4 Filtering and Moments

A common concept in the manipulation of cosmological density fields is that of filtering, which is just the convolution of the density field with some window function: $\delta \to \delta * f$ or in Fourier space $\delta_k \to \delta_k\ f_k$. The filtered power spectrum is $P(k)\,|f_k|^2$. Many observable results can be expressed in

this form. Two common 3D filter functions are: (i) a Gaussian, which in real space is:

$$f(r) = \frac{V}{(2\pi)^{3/2} R_{\rm G}^3}\, e^{-\frac{r^2}{2R_{\rm G}^2}}$$

and in Fourier space becomes:

$$f_k = e^{-\frac{k^2 R_{\rm G}^2}{2}}$$

and (ii) a spherical top-hat window function which in real space is

$$f(r) = \frac{3V}{4\pi R_{\rm T}^3} \quad (r < R_{\rm T})$$

and in Fourier space becomes

$$f_k(kR_{\rm T}) = \frac{3}{(kR_{\rm T})^3}\left[\sin(kR_{\rm T}) - (kR_{\rm T})\cos(kR_{\rm T})\right] = \frac{3j_1(kR_{\rm T})}{kR_{\rm T}}\,,$$

where j_1 is the spherical Bessel function.

We are often interested not in the convolved field in itself, but in its variance for use as a convenient statistic—an example might be the rms fluctuations in the number of objects in a cell. By the convolution theorem, this means that we are interested in the second moment of the power spectrum times the squared Fourier transform of the filter.

A commonly used parameter is σ_8, the filtered variance in spheres of radius $R_{\rm T} = 8\,h^{-1}\,{\rm Mpc}$ – roughly corresponding to the scale of massive galaxy clusters – given by:

$$\sigma_8^2 = \frac{V}{2\pi^2}\int \frac{dk}{k}\, k^3 P(k)\left|f(k\,8\,h^{-1}\,{\rm Mpc})\right|^2\,. \tag{14.26}$$

Remember that k in the power spectrum is the comoving wavenumber and this is why the factor h^{-1} appears in the scale. Current estimates of σ_8 (which can be obtained from e.g. cosmic shear surveys or the abundance of massive galaxy clusters) are in the range $\sigma_8 \simeq 0.7 - 1.1$.

14.5 Complications: Redshift Space Distortions and Biased Galaxy Formation

In order to interpret the observed 3D distribution of galaxies in terms of the underlying power spectrum of the matter distribution, we need to take

into account two further complications: peculiar velocities (relative to the Hubble flow) which affect our determination of distance from the measured galaxy redshifts, and the fact that light (i.e. galaxies) may not be unbiased tracers of the mass.

That is, even if we measure accurately the redshifts of many galaxies in a region on the sky, the result is not a true 3D picture. This is because we do not observe galaxies in 3D. Rather, we observe their angular position on the sky, θ, and redshift z (at the distances of interest there is no z-independent distance estimator). But redshift has two components: the cosmological component due to the expansion of the universe, and the Doppler effect of peculiar velocities:

$$1 + z \to (1 + z)(1 + v/c) \quad \text{or} \quad z = \frac{DH_0 + v}{c}$$

We can thus define a redshift space $\mathbf{s}$ which is a transform of the real (or proper) space $\mathbf{r}$, as follows:

$$s_1 = r_1 = \frac{zc}{H_0}\,\theta_1\,; \quad s_2 = r_2 = \frac{zc}{H_0}\,\theta_2\,; \quad s_3 = r_3 + \frac{v_3}{H_0}$$

It is the radial axis of redshift which is modified by the Doppler effects of peculiar velocities. The complication is that the peculiar velocities arise from the clustering itself. Thus, the apparent clustering pattern in redshift space differs systematically from that in real space and the spatial correlation function of galaxies, $\xi_g(\mathbf{r})$, which is isotropic in real space is no longer isotropic in redshift space.

There are two effects at work here. The first, termed the *'Fingers of God'* (see Fig. 14.1), is due to the velocity dispersion of galaxies within rich clusters and stretches out a cluster in redshift space. Since this affects only redshift and not position on the sky, the stretching occurs only radially (this is why the 'fingers' point back to observer). The other important redshift distortion is the Kaiser effect, due to galaxies bound to a central mass and still undergoing infall. It differs from the Fingers-of-God in that the peculiar velocities are coherent, not random, towards the central mass, though the effect is more subtle. The two effects are sketched in Fig. 14.7.

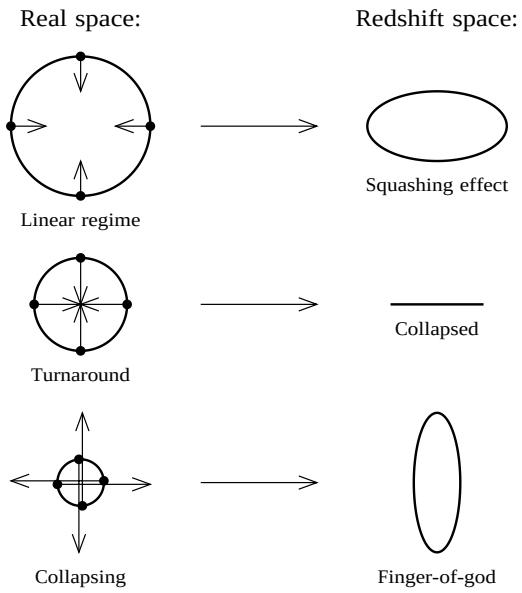

Figure 14.7: Redshift-space distortions

It can be shown that the redshift-space and real-space density fields are related via:

$$\delta_{\mathrm{m,z}} = \delta_{\mathrm{m,r}} \left[1 + f(\Omega_{\mathrm{m},0})\mu^2\right]$$

where μ is the cosine of the angle between the velocity vector and the line of sight, and $f(\Omega_{\mathrm{m},0}) \approx \Omega_{\mathrm{m},0}^{0.6}$ is the 'velocity suppression factor' proposed by Peebles.

The second complication arises from the fact that in galaxy redshift surveys we map out the distribution of the light, whereas we are interested in the mass density field. The relation between mass and light is determined by complex physical processes, but is generally described by a linear bias parameter b (that is, we assume some linear response of the galaxy formation process to small density perturbations), such that:

$$\delta_{\mathrm{lum}} = b \cdot \delta_{\mathrm{m}} = \delta_{\mathrm{m}} + (b-1)\,\delta_{\mathrm{m}}$$

The point of the trivial rearrangement is to emphasize that the observed density fluctuation is a mixture of the dynamically generated density fluctuation, plus an additional term due to bias, which populates different regions of space in different ways. The first term is associated with peculiar velocities, but the second is not—the enhancements in galaxy densities

are just some additional pattern.

In redshift space, we therefore add the anisotropic perturbations due to the dynamical component to the isotropic biased component, to obtain

$$\delta_{\rm lum,z} = \delta_{\rm m,r}\left[1 + f(\Omega_{\rm m,0})\mu^2\right] + (b-1)\delta_{\rm m,r} = \delta_{\rm lum,r}\left[1 + \frac{f(\Omega_{\rm m,0})\mu^2}{b}\right] \quad (14.27)$$

Redshift-space effects thus give us a characteristic anisotropy of clustering, which can be used to measure the parameter $\beta = \Omega_{\rm m,0}^{0.6}/b$. The power spectra in redshift and real space are related by:

$$\frac{P_z}{P_r} = \left(1 + \beta\mu^2\right)^2$$

14.6 Baryonic Acoustic Oscillations

Both the AAT 2dF and the SDSS teams announced in 2005 the discovery of a peak in $\xi(r)$ at $r \simeq 150\,{\rm Mpc}$ which they interpreted as the first evidence for acoustic peaks in the galaxy power spectrum (see Figures 14.6 and 14.8). The discovery, which had been anticipated a decade earlier, was heralded as a spectacular confirmation of the standard cosmological model in which mass overdensities grow from the seeds of CMB fluctuations. Since then, following these Baryonic Acoustic Oscillations (or BAO for short) over cosmic time has been a major motivation for reaching to ever-increasing size and depth in large galaxy surveys.

In Lectures 9 and 10 we discussed at length the conditions in the Universe around the epoch of recombination. We saw that, prior to recombination and decoupling, the Universe consisted of a hot plasma of photons and baryons which were tightly coupled via Thomson scattering. The competing forces of radiation pressure and gravity set up oscillations in the photon-baryon fluid. These oscillations left their imprint in the anisotropies of the CMB, emitted at $z_{\rm dec} = 1090$.

But what about the baryons? After decoupling, a baryon wave corresponding to an overdensity stalls. The radius reached at that point becomes imprinted on the distribution of baryons as a density excess. Since the baryons and dark matter interact though gravity, the dark matter also

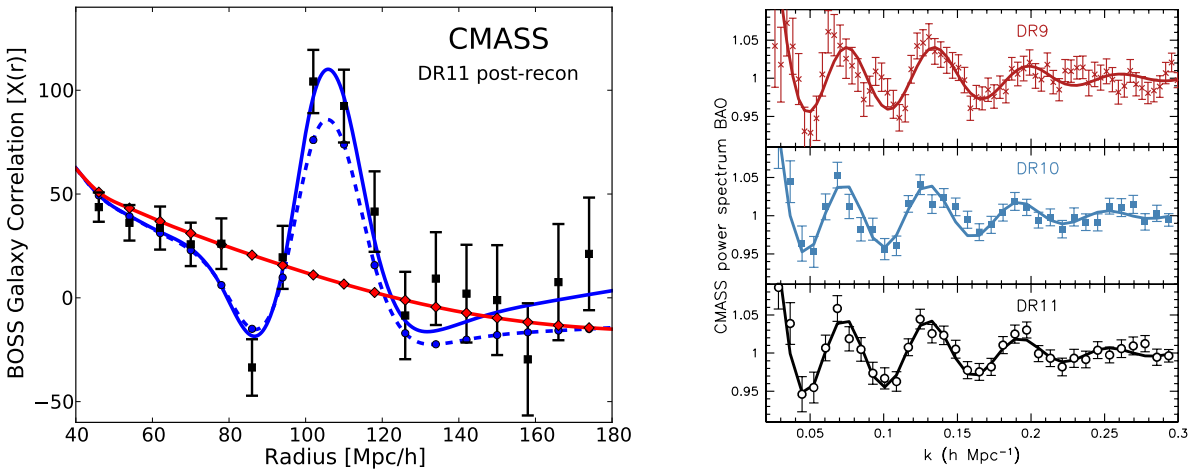

Figure 14.8: *Left:* Baryonic acoustic peak in the two-point correlation function of $\sim 10^6$ galaxies at redshifts $0.4 < z < 0.7$ as determined by the Baryon Oscillation Spectroscopic Survey (BOSS) project. The blue solid line is the best-fit BAO model, while the red line shows the fit by a model which does not include the BAO. *Right:* The BAO feature of the left panel is shown here in the power spectrum of the galaxy distribution: a spike in real space becomes a series of ripples in k-space. The results for three successive data releases of the BOSS project are shown separately. The data and the best fits have been normalised by dividing by the smooth model shown by the red continuous line in the left panel. (Figures reproduced from Anderson et al. 2014).

preferentially clumps on this scale. There is thus a increased probability that a galaxy will form somewhere in the higher density remains of the stalled baryon wave. The galaxy two-point correlation function would then show a 'bump' on this scale s, reflecting the higher probability of finding two galaxies separated by a distance s.

The scale s is usually close to the sound horizon, the comoving distance a sound wave could have travelled in the photon-baryon fluid by the time of decoupling. Given that the density of photons is much higher than the density of baryons, the photons decouple (i.e. they stop noticing the baryons) earlier than the baryons stop noticing the photons. The delay between the two is sometimes referred to as the 'baryon drag'. Defining the respective epochs as the time when the optical depth is one, $z_{\rm dec} = 1090$ for the photons (as we saw in Lecture 9), and $z_{\rm drag} = 1060$. The sound horizon at $z_{\rm drag}$ is $r_{\rm drag} = 147.4 \pm 0.3\,{\rm Mpc}$ (comoving), as determined from the analysis of the full set of Planck data.

14.6.1 Cosmological Parameters from BAO

We saw in Lecture 10.3.1 that the first Doppler peak in the CMB fluctuations acts as a cosmological *'standard ruler'* from which cosmological parameters can be deduced via the angular diameter distance. The position of the first peak is that expected for a flat Universe with $\Omega_{\rm k,0} = 0$.

The CMB anisotropies give us a measure of the angular extent of the sound horizon on the sky (at the surface of last scattering) at a single epoch, $z_{\rm dec}$. With the baryons, we can follow the evolution of the peak in BAO over cosmic times and thereby perform an analogous angular diameter distance test at different redshifts using $r_{\rm drag}$ as the standard ruler. We have already seen in Lectures 6 and 10 that it is the *combination* of different tests, with different sensitivities to the cosmological parameters, that allows us to reduce significantly the allowed parameter space for these parameters.

The use of BAO in this context has attracted a great deal of attention in the last ten years for the following reasons: (i) The scale $r_{\rm drag} \simeq 150\,{\rm Mpc}$ is sufficiently large that it remains in the linear regime to the present day; thus, the signal it produces in the large-scale distribution of galaxies is essentially insensitive to the astrophysical processes that occur on much smaller scales. (ii) BAO do not suffer from the systematic uncertainties that potentially limit the progress that can be made with Type Ia supernovae (Lecture 6), in particular the possibility that the relations between colour, luminosity and light curve shape may not be entirely constant with look-back time. Recall that we do not yet have an established physical model for Type Ia explosions: their use as 'standard candles' is based entirely on empirical considerations.

On the other hand, the small amplitude of the baryon acoustic peak and the large size of the relevant scales imply that volumes of many ${\rm Gpc}^3$ must be probed and samples of many hundreds of thousands of galaxies must be assembled in order to follow the peak over a range of redshifts.

With BAO, it is possible (after correction for the effects described in Section 14.5) to determine the angular diameter distance and the Hubble rate separately, by measuring the clustering scale s respectively *along* the line of sight (via redshift measurements) and *tangentially* on the sky (see Fig-

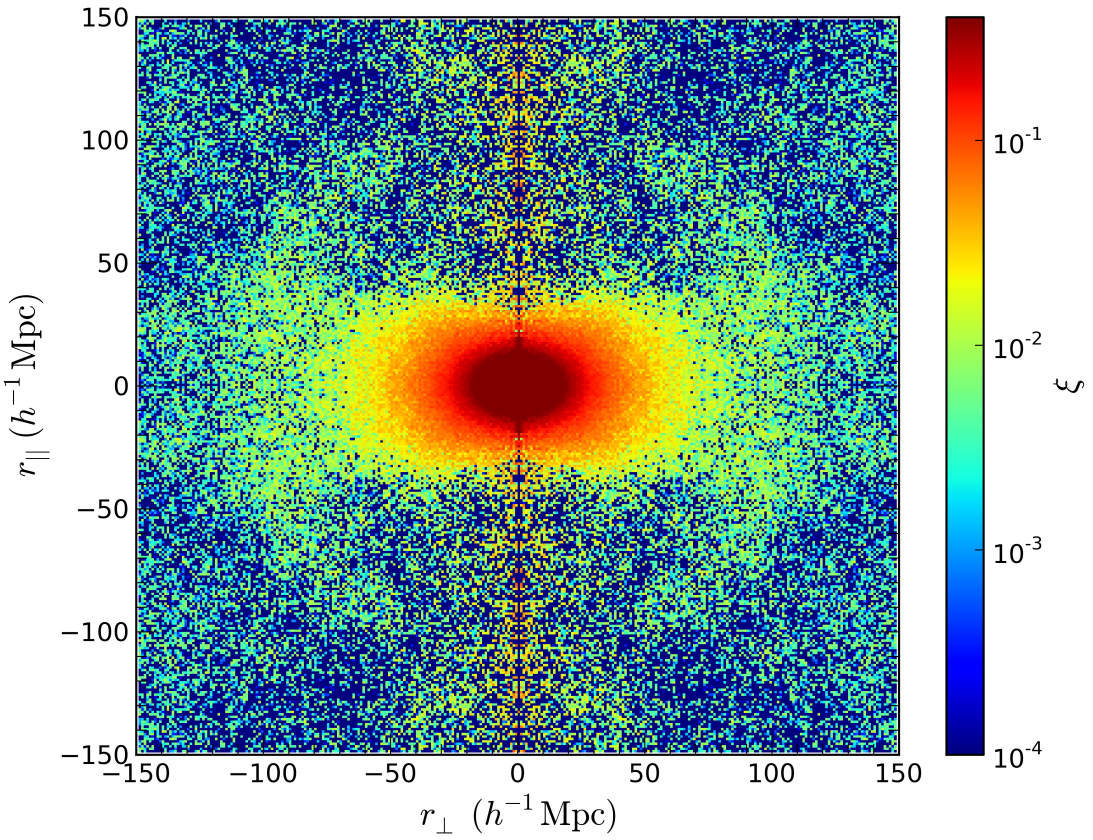

Figure 14.9: The two-dimensional correlation function of galaxies in the BOSS sample in bins of $1h^{-1} \times 1h^{-1}\,\mathrm{Mpc}^2$. The ring of slightly enhanced clustering at $r_\parallel = r_\perp \simeq 100h^{-1}\,\mathrm{Mpc}$ is the BAO signal. (Figure reproduced from Samushia et al. 2014).

ure 14.9). Specifically:

$$H(z) = \frac{c\,\Delta z}{s_\parallel(z)} \tag{14.28}$$

and

$$d_\mathrm{A}(z) = \frac{s_\perp}{\Delta\theta\,(1+z)}\,. \tag{14.29}$$

Both $H(z)$ and $d_\mathrm{A}(z)$ depend on the cosmological parameters $\Omega_{\mathrm{m},0}$, $\Omega_{\mathrm{k},0}$, and $\Omega_{\Lambda,0}$ (eqs. 5.12 and 5.34). Thus, the possibility that by tracking the BAO feature from the present time to $z \sim 1$ may yield clues to the nature of dark energy, which takes over cosmic expansion during this epoch, has motivated huge galaxy surveys in the last decade. Two of the largest are the AAT WiggleZ survey and the SDSS BOSS project, each consisting of hundreds of thousands of galaxy redshifts out to $z \sim 1$.

In Figure 14.10 we show joint constraints from these projects on the parameters H_0, $\Omega_{\mathrm{m},0}$ and $\Omega_{\mathrm{k},0}$. Figure 14.11 shows confidence contours for the dark energy equation of state parameter w ($p = w\rho$), where p is the pressure and ρ is the density—see Lecture 6.4), assumed to be a constant

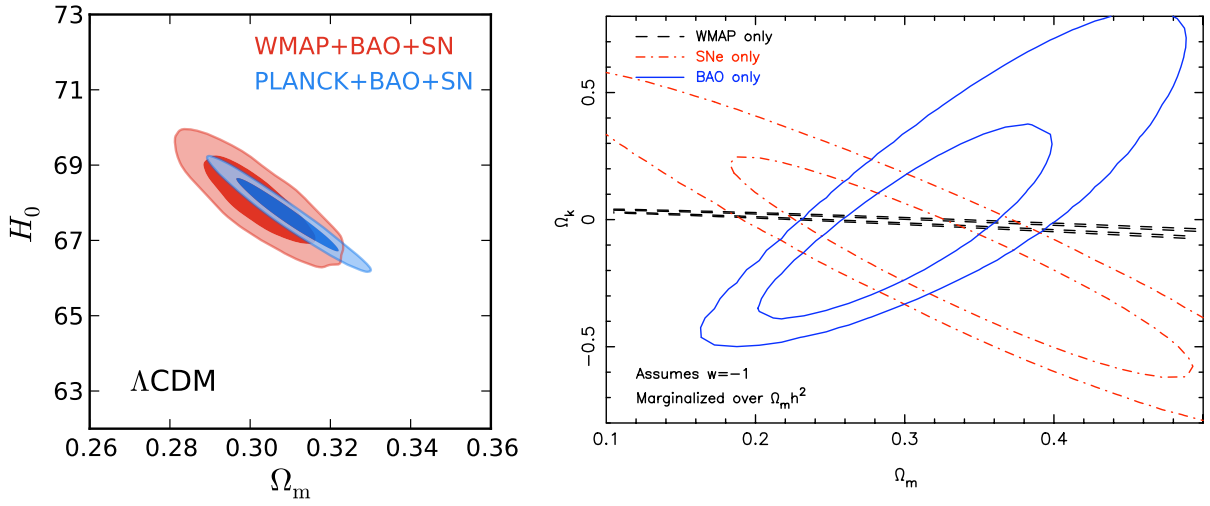

Figure 14.10: *Left:* Joint probability contours (68% and 95%) on H_0 and $\Omega_{\mathrm{m},0}$ obtained by combining the BOSS BAO with measurements with CMB and SN data (Figure reproduced from Anderson et al. 2014). *Right:* Probability contours between $\Omega_{\mathrm{k},0}$ (y-axis) and $\Omega_{\mathrm{m},0}$ (x-axis) shown separately for CMB (WMAP), BAO (WiggleZ) and SN data, illustrating the complementarity of the three techniques (Figure reproduced from Blake et al. 2011).

in the left panel, and assumed in the right panel to be a simple function of the scale factor a:

$$w(a) = w_0 + w_a\,(1-a)\,, \tag{14.30}$$

as already considered in Lecture 6.4.

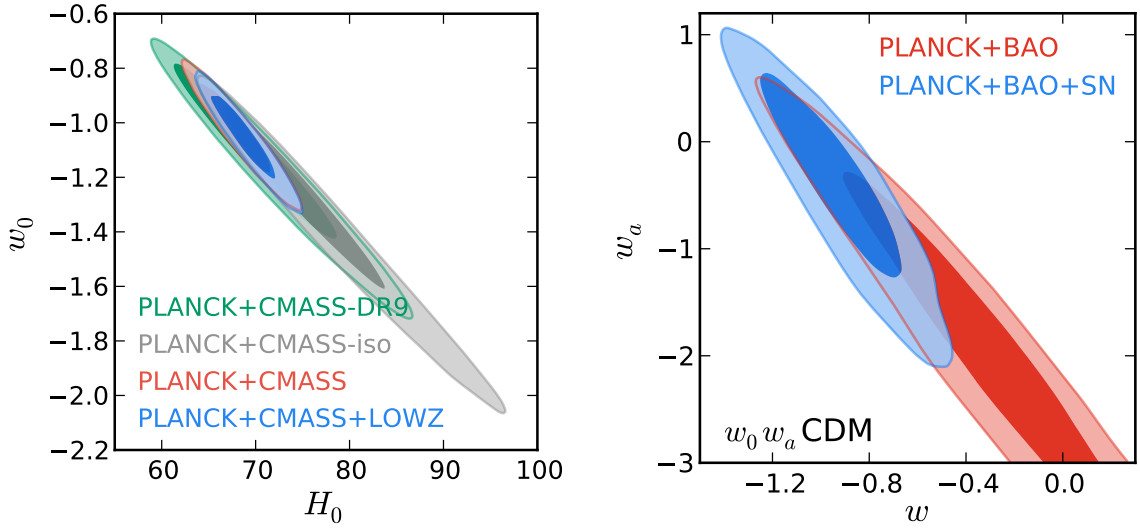

Figure 14.11: *Left:* Probability contours in the w and H_0 obtained by combining BOSS BAO with Planck CMB observations, showing the degeneracy between the Hubble constant and the dark energy equation of state. *Right:* Constraints on a varying equation of state parameter according to eq. 14.30 from BAO+CMB, as indicated. (Both figures reproduced from Anderson et al. 2014).

The outcome of all of these tests is the 'precision cosmology' which we discussed at the beginning of this course (Table 1.1). In particular, note that no evidence has been found yet to support suggestions that dark energy is anything more than Einstein's cosmological constant; the BOSS results reproduced in Figure 14.11 are entirely consistent with $w_a = 0$, $w_0 = -1$. As can be seen from Figure 14.12, the cosmic distance scale indicated from the SN observations is in excellent agreement with that deduced from BAO.

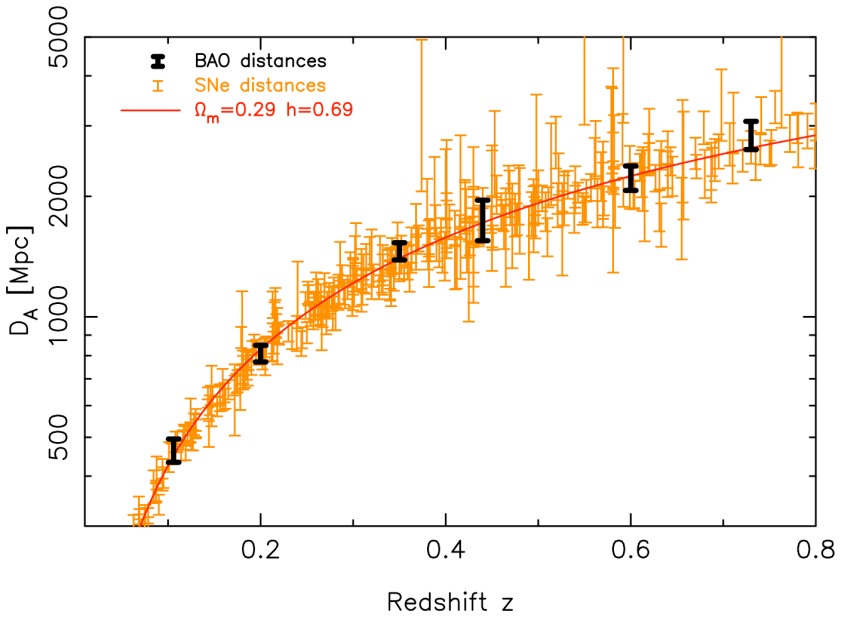

Figure 14.12: Comparison between the SN and BAO mapping of the cosmic distance scale. For the purpose of this figure, the SN $d_{\rm L}$ measurements have been converted to $d_{\rm A}$, assuming $d_{\rm A}(z) = d_{\rm L}(z)/\left(1+z\right)^2$ (Figure reproduced from Blake et al. 2011).

14.7 The Matter Power Spectrum

The large scale distribution of galaxies traces the matter power spectrum on scales of 10s to 100s of Mpc. This is only part of the story, however. As illustrated in Figure 14.13, cosmic structure has now been probed over four orders of magnitude, from scales of a few Mpc via the intergalactic Lyman alpha clouds we studied in Lectures 12 and 13, through scales of $\sim 10\,$Mpc using weak gravitational lensing (to be introduced in Lecture 16), to scales of $\sim$ 1–10 Gpc with the CMB fluctuations that were the subject of Lecture 10.

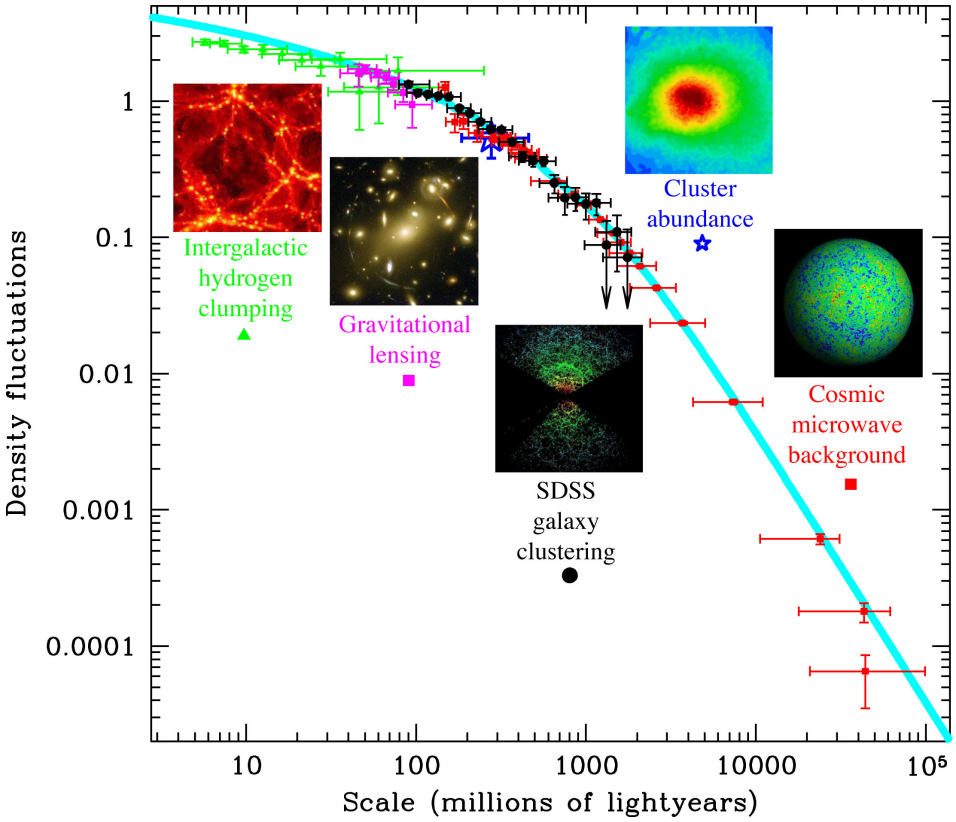

Figure 14.13: The power spectrum of density fluctuations in the Universe. The y-axis scale, labelled 'Density fluctuations', shows $\Delta^2(k) \propto k^3 P(k)$ (eq. 14.18), while the x-axis is the comoving scale (1 Mpc $\sim$ 3.3 Mly). Different tracers of the density are used on different scales. The turquoise curve shows a fit to the data with the parameters of the standard ΛCDM cosmological model (Figure credit: Max Tegmark, MIT).

Max Tegmark's website (http://space.mit.edu/home/tegmark/movies.html) has a hands-on tool which allows one to see directly the effect of varying cosmological parameters on the shape and normalisation of $P(k)$.